Using Atom-Probe Tomography to Understand ZnO:Al/SiO_2/Si Schottky Diodes

R. Jaramillo,[1,*] Amanda Youssef,[2] Austin Akey,[2] Frank Schoofs,[3] Shriram Ramanathan,[3,4] and Tonio Buonassisi[2]

[1]*Department of Materials Science and Engineering, Massachusetts Institute of Technology, 77 Massachusetts Avenue, Cambridge, Massachusetts 02139, USA*

[2]*Department of Mechanical Engineering, Massachusetts Institute of Technology, 77 Massachusetts Avenue, Cambridge, Massachusetts 02139, USA*

[3]*School of Engineering and Applied Sciences, Harvard University, 9 Oxford Street, Cambridge, Massachusetts 02138, USA*

[4]*School of Materials Engineering, Purdue University, West Lafayette, Indiana 47907, USA*

(Received 13 November 2015; revised manuscript received 25 July 2016; published 26 September 2016)

We use electronic transport and atom-probe tomography to study ZnO:Al/SiO_2/Si Schottky diodes on lightly doped *n*- and *p*-type Si. We vary the carrier concentration in the ZnO:Al films by 2 orders of magnitude, but the Schottky barrier height remains nearly constant. Atom-probe tomography shows that Al segregates to the interface, so that the ZnO:Al at the junction is likely to be metallic even when the bulk of the ZnO:Al film is semiconducting. We hypothesize that the observed Fermi-level pinning is connected to the insulator-metal transition in doped ZnO. This implies that tuning the band alignment at oxide/Si interfaces may be achieved by controlling the transition between localized and extended states in the oxide, thereby changing the orbital hybridization across the interface.

DOI: 10.1103/PhysRevApplied.6.034016

I. INTRODUCTION

The electron energy band alignment at the interface between oxides and Si is critical for several technologies. Examples include the development of alternative gate dielectrics for continued field-effect transistor scaling, and the development of carrier-selective contacts with wide band gaps for Si heterojunction solar cells [1–4]. All such applications would benefit from controlling the band offset at the oxide/Si interface. Here, we consider what happens when the oxide is electrically conductive. For the interface between conventional metals and Si the band alignment is weakly dependent on the metal work function [5]. Schottky barrier-height measurements show that the Fermi energy (E_F) at the interface is usually fixed (or "pinned") in the lower half of the Si band gap. We ask two related questions: Will replacement of the metal by an oxide that can be tuned across an insulator-metal transition shed light on the phenomenon of Fermi-level pinning? Will it allow greater control over the band alignment?

Many theoretical concepts have been proposed to explain Schottky barrier-height pinning [6–11]. Semiconductor band bending is well understood, and the long-range (100 nm or more) electrostatics of Schottky barriers are rarely in question. The proliferation of theoretical concepts stems from an uncertainty over the short-range electrostatics and the origin of dipoles that shift the Fermi level. Explanations for these dipoles include the charging of surface states, the spontaneous formation of charged point defects, the existence of metallic secondary phases at the interface, the formation of polar bonds across the interface, and charge transfer due to orbital hybridization across the interface. This last concept includes metal-induced gap states (MIGS) in the semiconductor, but has been shown to be more general [6–11]. Despite decades of study, probably the most general statement that can be made about Schottky barriers is that theories must be continuously reevaluated in the light of material-specific details [6].

We use electronic transport measurements to determine the band alignment at ZnO:Al/SiO_2/Si Schottky diodes for a range of carrier concentrations in the ZnO:Al (AZO) film, and we use atom-probe tomography (APT) to measure the atomic composition at the interface. Our results suggest that the pinning of E_F in the lower half of the Si band gap at the interface is connected to the insulator-metal transition in ZnO. This lends experimental support to the concept of orbital hybridization and MIGS, wherein extended electronic states in the metal hybridize with the semiconductor, leading to a net transfer of charge and an interface dipole [6,10,12]. We hypothesize that the band alignment could be tuned by controlling the transition between localized and extended states in the oxide, thereby changing the orbital hybridization across the interface. Experimental control over this process is inhibited by chemical segregation, and this compositional heterogeneity presents an obstacle to device engineering.

AZO offers a large synthesis-properties-performance parameter space, and key properties such as work function, carrier concentration, mobility, and optical band gap can be controlled by the film-synthesis conditions [13]. The work function of AZO and other ZnO-based transparent conductors has been reported to vary from 4.2 to 5.1 eV

*rjaramil@mit.edu

[13–15]. This could be naively interpreted as meaning that the Schottky barrier height (Φ) at an AZO-semiconductor junction could be tuned by 0.9 eV. However, most reported work-function measurements were performed on the exposed surface of AZO films. Moreover, Schottky barrier heights at metal-Si heterojunctions are only weakly dependent on the metal work function. Schottky barriers depend on interface-specific dipoles, and therefore we expect that the work function of exposed surfaces of AZO films will not be directly relevant to the AZO/SiO_2/Si Schottky barrier height.

II. DESCRIPTION OF EXPERIMENT

We synthesize AZO/SiO_2/Si Schottky diodes by reactive sputtering of AZO films on Si wafers. We deposit on both *n*- and *p*-type Si substrates with carrier concentrations of $(4.1 \pm 1.5) \times 10^{15}$ cm^{-3} and $(2.2 \pm 0.5) \times 10^{15}$ cm^{-3}, respectively, as measured by Mott-Schottky capacitance profiling. Before AZO deposition the substrates are prepared by forming a thin controlled SiO_2 layer, in order to avoid uncontrolled SiO_2 formation during the AZO sputtering process. The SiO_2 layer is 15 ± 2 Å thick as measured by ellipsometry. We simultaneously deposit witness films on glass slides and on oxidized Si wafers for measurements of electrical resistivity, Hall resistivity, optical spectroscopy, and x-ray diffraction.

We control the AZO film properties by changing the oxygen gas flow into the growth chamber. We use the transparent conductor figure of merit as a metric to define the oxygen content in the films [14]. Oxygen-poor films are conductive but not transparent, and oxygen-rich films are transparent but not conductive. The oxygen content is measured as a percentage of oxygen flow relative to the optimal film, and we write this relative oxygen content as R_{O_2}. Hall measurements show that the free-electron concentration at room temperature varies from $(8.2 \pm 0.3) \times 10^{20}$ cm^{-3} for oxygen-poor films to $(1.14 \pm 0.05) \times 10^{19}$ cm^{-3} for oxygen-rich films. For samples that are nonuniform in the out-of-plane direction, the Hall data should be analyzed using a model including multiple conduction channels. Since this would result in the model parameters being underdetermined, we use a single-channel model instead. As discussed below, we suggest that in the immediate vicinity of the substrate the carrier concentration of the film is enhanced. In this case, analyzing the Hall data in terms of a single channel will overestimate the free-electron concentration in the film farther from the interface. The overestimate is likely to be small for most of the samples discussed here [16].

The critical free carrier concentration for the insulator-metal transition between localized and extended electronic states for ZnO is in the range of $(5–8) \times 10^{19}$ cm^{-3}, meaning that our study includes semiconducting and

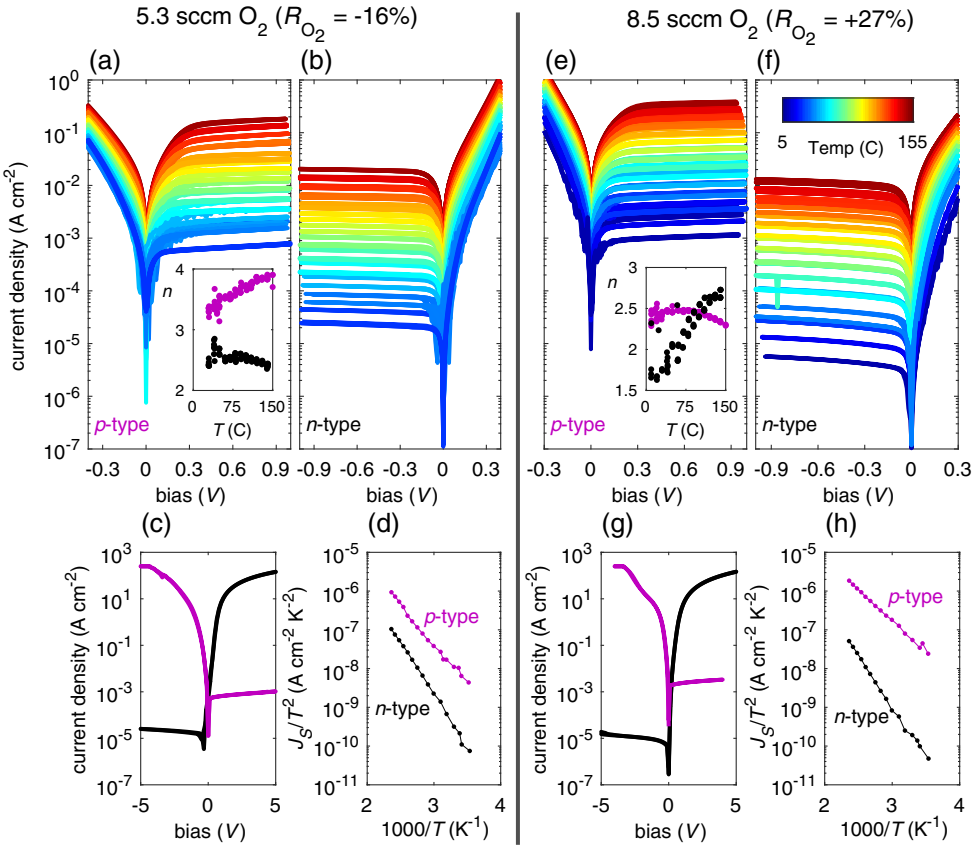

FIG. 1. Measuring Schottky barrier heights. We show $J(V,T)$ data and activation energy plots for two AZO compositions, oxygen poor ($R_{O_2} = -16\%$, left half) and oxygen rich ($R_{O_2} = 27\%$, right half). (a), (e) and (b), (f) Data for samples on *p*-type and *n*-type Si, respectively. The measurement T is represented by the line color according to the color bar in (f). [(a) and (e), insets] The diode ideality factors for *p*-type (purple) and *n*-type (black) samples. (c), (g) Data at room T measured over a wider bias range. (d), (h) The saturation current density (J_S) shown as an activation energy plot. The slope of these lines yields the barrier height.

metallic samples [31]. This is confirmed by temperature-dependent measurements of the resistance (R) that show $d\ln(R)/dT \geq 0$ for oxygen-poor and optimal samples, and $d\ln(R)/dT < 0$ for oxygen-rich samples [16]. The $R(T)$ data suggest that the insulator-metal transition occurs in the range $0 < R_{O_2} < 15\%$, somewhat lower than the transition range suggested by Hall measurements. This is consistent with the overestimation of the free-electron concentration by using a single conduction channel model to analyze the Hall data.

We determine Φ by measuring current-voltage [$J(V)$] curves as a function of temperature (T), and analyzing the reverse saturation current density [$J_S(T)$]. In Fig. 1 we show representative $J(V)$ data and analysis for 2 of the 26 samples in this study. Each $J(V)$ curve is used to determine the saturation current density (J_S) at that particular temperature. J_S can be determined by fitting the data to a diode model; because our samples show low current leakage due to shunt resistance, and J_S can also be determined by the unprocessed $J(V)$ at reverse bias. Either approach leads to quantitatively consistent results for Φ. The ideality factor (n) determined by fitting our data to a single diode model depends on temperature and varies between 1.5 and 4 for all samples reported here. This large and temperature-dependent ideality factor is consistent with metal-insulator-semiconductor junctions with polycrystalline thin films, as opposed to intimate, epitaxial, metal-semiconductor junctions [6]. In Figs. 1(d) and 1(h) we show J_S/T^2 plotted as a function of T^{-1}. This is an activation energy plot, and the slope determines Φ [5]. The fact that the activation energy plots are straight lines over many decades of J_S/T^2 justifies the use of the theory of thermionic emission to model the data.

We use APT to provide three-dimensional chemical-composition analysis of the interface with atomic resolution. The APT samples are prepared from the same Schottky diodes that are used for electrical measurements. Please see the Supplemental Material for full details [16].

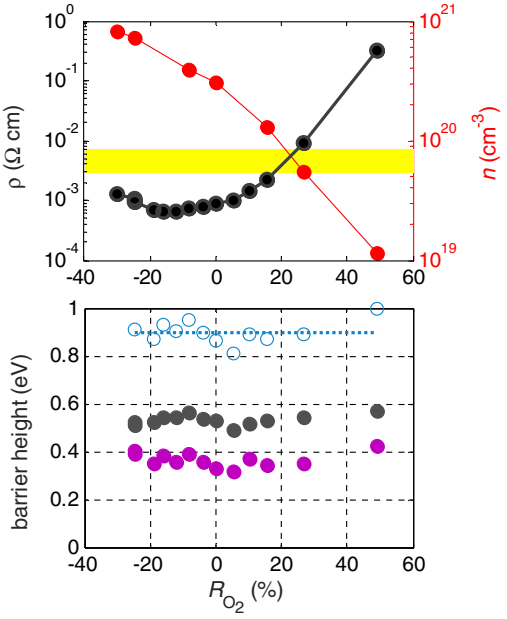

FIG. 2. AZO film properties and Schottky barrier heights on n- and p-type Si. (a) Resistivity (left axis, black curve) and conduction electron concentration (right axis, red curve) for AZO films as a function of relative oxygen content R_{O_2} (see text). The yellow bar indicates the electron concentration corresponding to the insulator-metal transition in ZnO [31]. (b) Schottky barrier height for $AZO/SiO_2/Si$ diodes on both n-type (black points) and p-type (purple points) Si. The sum of barrier heights $\Phi_n + \Phi_p$ is shown in light blue.

III. RESULTS

We find that Φ is independent of AZO film properties for both n- and p-type diodes. We plot the AZO carrier concentration in Fig. 2(a) and the measured barrier heights

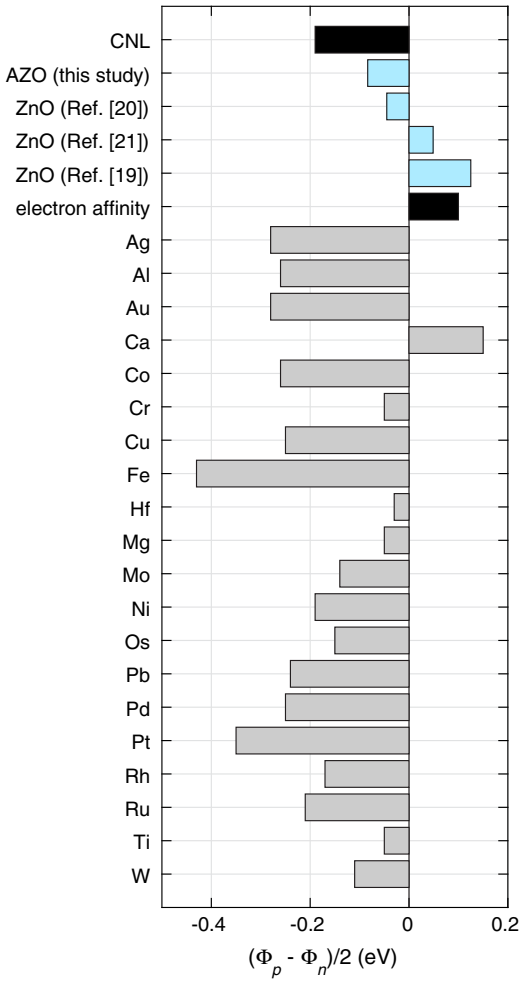

FIG. 3. We compare the difference $(\Phi_p - \Phi_n)/2$ found here to that reported in the literature for metals and ZnO, and to predictions of barrier heights based on charge neutrality level (CNL) and electron affinity rules of band alignment [5,32–35]. See Supplemental Material for details including the work function of ZnO and treatment of results in Ref. [35] [16].

in Fig. 2(b). E_F is consistently found at $\Phi_p = 0.37 \pm 0.03$ eV above the valence band edge (E_V) for p-type diodes, and $\Phi_n = 0.53 \pm 0.02$ eV below the conduction band edge (E_C) for n-type diodes. Here and throughout, Φ_p and Φ_n are the barrier heights measured on p- and n-type diodes, respectively. These values underestimate the actual Schottky barrier heights. This is clear from the sum $\Phi_p + \Phi_n = 0.90 \pm 0.05$ eV, which is lower than the Si band gap ($E_g^{\mathrm{Si}} = 1.1$ eV). There are two reasons for this. First, our samples are metal-insulator-semiconductor (M-I-S) diodes and our analysis does not account for image-charge lowering or for the voltage across the SiO_2 layer [5]. Second, most Schottky diodes are spatially nonuniform, and measurements of J_0 are disproportionately affected by regions of low Φ [6]. If we assume that Φ is lowered equally for n- and p-type diodes, then E_F is 0.47 eV above E_V for p-type samples, and 0.63 eV below E_C for n-type samples.

In Fig. 3 we compare our estimate $(\Phi_p - \Phi_n)/2 = -0.084$ eV to the expectations for Fermi-level pinning at the charge neutrality level (CNL), for an idealized Schottky junction (electron affinity alignment), and to previously published results on metal/Si and ZnO/Si diodes [5,32–35]. With the exception of Ca, AZO/Si, and metal/Si diodes all exhibit $\Phi_n > \Phi_p$, meaning that the Fermi level at the interface is in the lower half of the Si band gap. We also show the value expected for an idealized ZnO/Si diode, for which Φ_p and Φ_n are determined by the work function of ZnO (taken here as 4.5 eV) [16]. In this case the order is reversed, $\Phi_n < \Phi_p$. There are several published reports of ZnO/Si diodes for which barrier-height measurements were made on both n- and p-type substrates, and these results are reproduced in Fig. 3. The ZnO/Si diode results cover both $\Phi_n > \Phi_p$ and $\Phi_n < \Phi_p$. The band alignment for undoped ZnO closely matches the prediction for an idealized Schottky junction [33]. Evidently, the band alignment between ZnO and Si can be tuned by doping. We hypothesize that the mechanism that creates a dipole at the AZO/Si interface is not present at the ZnO/Si interface, and that this mechanism is connected to the electrical conductivity of AZO. However, the carrier concentration and conductivity vary widely across our sample set, which includes samples on the semiconducting side of the insulator-metal transition, and yet the Fermi level remains fixed.

Band offsets are affected by dipoles that are confined to the interface. To understand our device results we use APT to study the composition of our interfaces with atomic resolution. In Fig. 4 we show two-dimensional contour lines of the three-dimensional Al concentration data. The overall Al concentration decreases with increasing oxygen content, as expected from point-defect thermodynamics [36]. There is a significant segregation of Al to the

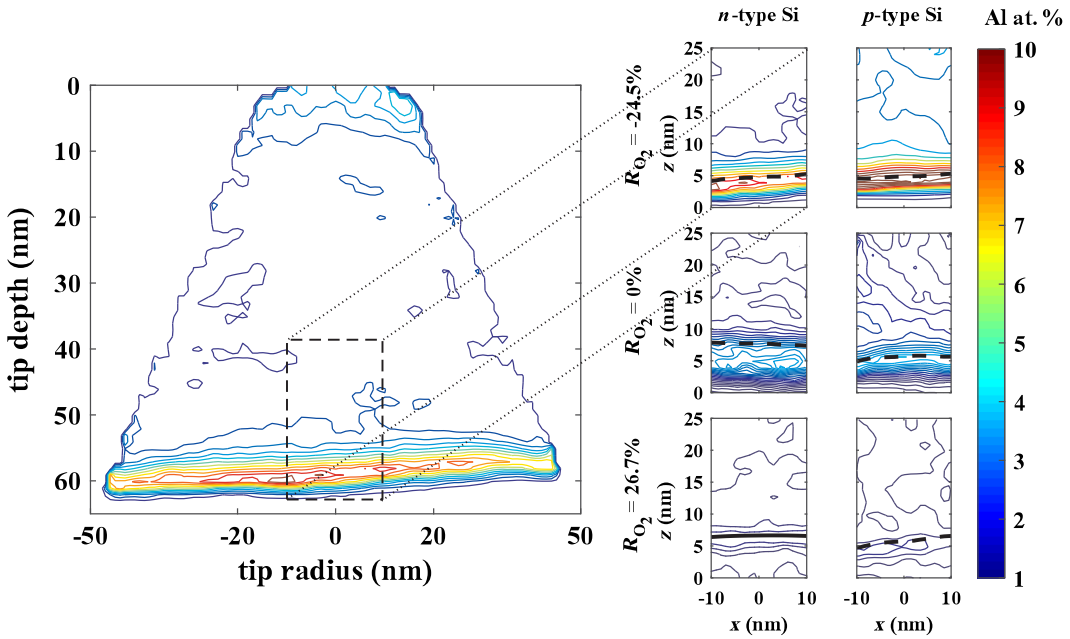

FIG. 4. Al segregation at the AZO/SiO_2/Si interface observed by APT. (Left) 2D contour plot of the Al concentration (at. %) for the oxygen-poor ($R_{O_2} = -24.5\%$) AZO layer on n-type Si substrate. The 2D projection from the entire tip volume contour plots is generated by sampling the 3D grid in the z direction with a distance between the sampling planes equal to 1 nm. (Right) 2D contour plots of the Al concentration for all six samples measured by APT. The dashed black line corresponds to the defined interface (5 at. % Si). 3D reconstruction artifacts such as curvature effects are caused by the difference in evaporation field needed to field evaporate the different elements present at the junction and the resulting change in the image compression factor. Also, notice the interface line being tilted, this is the result of sample preparation wherein the tip is deposited slightly offset from its vertical position. The measured Al concentrations are systematically inflated because the oxygen content cannot be accurately measured [16].

$AZO/SiO_2/Si$ interface for all samples, as also observed by Bikowski *et al.* [37]. This suggests that at the interface the AZO is always highly doped, even for films that are semiconducting in the bulk.

The APT data can be reduced to one dimension through the use of a proximity histogram ("proxigram") by averaging over planes perpendicular to the interface, which reduces distortions caused by curvature artifacts in the reconstruction. The interface is defined as the depth at which Si reaches 5 at. % [16]. The measured Al concentrations are systematically inflated because the oxygen content cannot be accurately measured (because O_2^{2+} and O^{1+} are indistinguishable). As a result, the measured $(Zn + Al):O$ ratios are nearly 2:1 throughout the AZO films [16]. As a correction, we scale the metal concentrations such that the ratio $(Zn + Al):O$ is 1:1 in the midst of the AZO layer. We plot the resulting Al composition profiles in Fig. 5(a).

Conduction electrons (e' in Kröger-Vink notation) in AZO come from ionized donors $Al_{Zn}^{\cdot}$. The corresponding Brouwer approximation is that $[Al_{Zn}^{\cdot}] = [e']$. Our AZO films are all n type, and Al_{Zn} is the donor with the lowest formation energy in both the oxygen-poor and oxygen-rich limits [36]. Therefore, we assume that the same Brouwer approximation applies for our full sample set. It is likely that Al exists in forms other than $Al_{Zn}^{\cdot}$ in our films, and the distribution of Al in its different forms would be sample dependent (due to dependencies on oxygen content). Therefore, we assume a simple relationship between the concentration of ionized donors and the total Al concentration through a film-dependent factor f: $[Al_{Zn}^{\cdot}] = f[Al]$. Hall measurements give $[e']$ typical of the through thickness of the film, and APT data give us [Al] far from the interface. Thereby, we determine f for each sample, and use it to calculate $[Al_{Zn}^{\cdot}]$ through the interface. We plot the results in Fig. 5(b). For the semiconducting oxygen-rich film, the apparent concentration of ionized donors at the interface is sufficiently high as to cross the insulator-metal transition, leading to metallic conduction at the interface. The assumption that the factor f is constant for a given sample overlooks the fact that the ionized fraction $[Al_{Zn}^{\cdot}]/[Al]$ could change with the local environment, and therefore the curves in Fig. 5(b) should be considered upper bounds on the local carrier concentration.

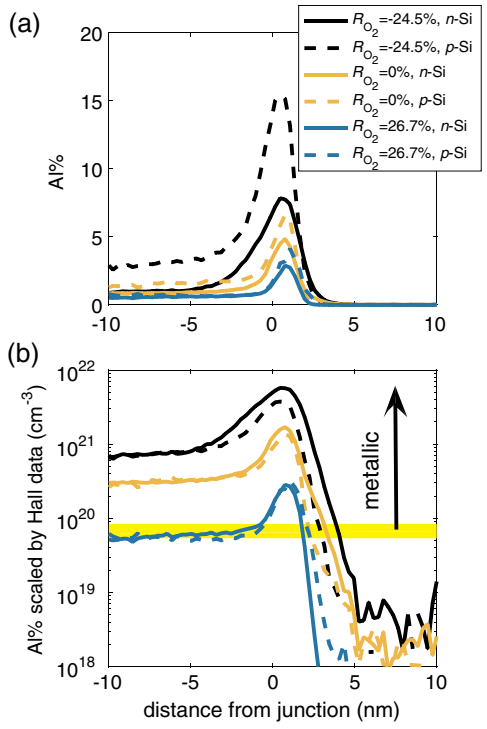

FIG. 5. Al concentration across the $AZO/SiO_2/Si$ interface, generated using a proxigram normal to an interface defined as 5 at. % Si. n-type samples are shown with solid lines, p-type samples are shown with dashed lines. Black, oxygen poor ($R_{O_2} = -24.5\%$). Orange, optimal ($R_{O_2} = 0\%$). Blue, oxygen rich ($R_{O_2} = 26.7\%$). (a) Al at. %. (b) Al concentration scaled by the Hall data measured on witness AZO films. The yellow bar indicates the free-electron concentration at the insulator-metal transition. The segregation of Al suggests that the concentration of ionized donors $Al_{Zn}^{\cdot}$ at the interface is always on the metallic side of the insulator-metal transition.

IV. DISCUSSION AND CONCLUSION

The APT data suggest that, at the interface, all of our films are on the metallic side of the insulator-metal transition, and that this is responsible for pinning the Fermi level. The exact composition at the interface varies from film to film, and yet the barrier heights remain nearly constant within the experimental error. There are small trends in the Φ_p and Φ_n data for $AZO/SiO_2/Si$ diodes that indicate some tuning of the barrier height (Fig. 2), but these trends are overwhelmed by the change in band alignment on going from ZnO to AZO as seen by comparing our results to those of Refs. [33–35] (Fig. 3). It seems that the proximity of a highly doped ZnO layer to the Si is sufficient to pin the Fermi level in the lower half of the Si band gap.

Device transport results show that the band alignment of ZnO/Si diodes can be changed by doping, and atom-probe results suggest that the AZO films are metallic at the interface, even for films that are semiconducting on average. Since our samples are M-I-S structures, there is no intimate contact between the metal (AZO) and the Si. The intrinsic layer is thin enough to allow electron tunneling between AZO and Si. These results suggest that the interface dipole is related to hybridization between extended, metal-derived states and the semiconductor. This is conceptually similar to the MIGS model, although we emphasize that detailed calculations are necessary to determine whether the energy of the resulting charge-transfer states lies in the semiconductor band gap [6].

Microscopic experimental evidence for MIGS contributing to the interface dipole has been shown for an intimate Fe/GaAs interface [12]. On the other hand, a layer of NiO

26 Å thick can reduce the interface dipole at metal/NiO/Si Schottky junctions; this is significantly thicker than the SiO_2 layer used here [4]. Taken together with our data, these results call for further study of the role of a thin intrinsic layer in modifying orbital hybridization, MIGS, and Fermi-level pinning in *M-I-S* Schottky diodes.

We suggest that the Schottky barrier height on Si could be modified by fine control of the carrier concentration at an insulator-metal transition, thereby affecting the density of extended electronic states. Such fine control is inhibited in AZO by the segregation of Al to the interface. Therefore, achieving a tunable barrier height in ZnO/Si junctions may depend on suppressing the mechanism that causes defect segregation at the interface. Theory predicts that Al dopants in ZnO are thermodynamically likely to segregate to grain boundaries and the surfaces of small crystals, but the applicability of these results to a buried interface between different materials is unclear [38,39]. Kinetic and/or electrostatic control of the interface during AZO growth may enable the desired control of defect segregation and thereby the insulator-metal transition.

APT measures composition but does not uniquely determine the phases present at the interface. The concentration of Al at the interface exceeds the solid solubility limit of 2% Al/Zn (equal to $[\mathrm{Al}] = 8.3 \times 10^{20}$ cm^{-3}), making more likely the presence of Al-rich secondary phases. We don't think that a metal alloy such as Al:Si would form, because the proximity to SiO_2 and the oxidizing growth environment mean that Al-rich oxides are strongly favored thermodynamically over Al-rich non-oxides. This makes it unlikely that the AZO/SiO_2/Si Schottky barrier heights here are fixed by the work function of metallic Al, as in the so-called effective work-function model for Schottky barriers on III–V semiconductors [8]. The presence of insulating Al_2O_3 or $ZnAl_2O_4$ as secondary phases at the SiO_2/AZO interface has been confirmed by a combination of transmission electron microscopy and transmission electron microscopy [37]. It is hypothesized that the low vapor pressures of Al, Al_2O_3, and $ZnAl_2O_4$ relative to Zn may be responsible for preferential deposition of Al-rich oxides during the early stages of film growth. This is a separate mechanism proposed to explain excess Al at the interface, in addition to the thermodynamic driving forces described by theory [37–39]. The presence of Al-rich oxides at the interface could affect the measured J_0, Φ_n, and Φ_p. A continuous Al_2O_3 or $ZnAl_2O_4$ film in between SiO_2 and AZO would increase the thickness of the intrinsic layer in our *M-I-S* devices, which would lower both Φ_n and Φ_p. In particular, this could be responsible for some of the observed sample-to-sample variation in $\Phi_n + \Phi_p$. Discontinuous patches of Al_2O_3 or $ZnAl_2O_4$ in between SiO_2 and AZO could lower J_0 without affecting the T-dependent diode analysis. In this case, the metallic interface layer would not be laterally uniform, and conduction through the film could be affected by percolation.

In summary, we show that the Fermi level is pinned in the lower half of the Si band gap at AZO/SiO_2/Si Schottky diodes, and we suggest that this is connected to the insulator-metal transition in AZO. Control of the diode is inhibited by the segregation of Al to the interface. We suggest that the ZnO/Si barrier height could be tuned by engineering point-defect distributions in order to continuously tune the insulator-metal transition at the interface. Doing so will require kinetic and/or electrostatic control of the interface during AZO growth to overcome the thermodynamic driving force for segregation. We emphasize the need to combine device transport with appropriate microscopy to better understand electronic heterojunctions. It would be particularly interesting to use high-resolution transmission electron microscopy combined with electron-energy-loss spectroscopy to measure the bulk plasmon energy, and thereby the free carrier concentration at the interface.

ACKNOWLEDGMENTS

We acknowledge Harry Tuller and Michael Campion for conversations and for sharing unpublished data. R. Jaramillo acknowledges the support of a Department of Energy (DOE) EERE Postdoctoral Research Award. This work was supported by the Bay Area Photovoltaic Consortium under DOE Contract No. DE-EE0004946. We acknowledge support from the Air Force Office of Scientific Research under Contract No. FA9550-12-1-0189, and from the National Science Foundation under Contract No. DMR-0952794. This work was performed in part at the Center for Nanoscale Systems (CNS), a member of the National Nanotechnology Infrastructure Network (NNIN), which is supported by the National Science Foundation under Contract No. ECS-0335765.

[1] C. J. Först, C. R. Ashman, K. Schwarz, and P. E. Blöchl, The interface between silicon and a high-k oxide, Nature (London) **427**, 53 (2004).

[2] A. M. Kolpak, F. J. Walker, J. W. Reiner, Y. Segal, D. Su, M. S. Sawicki, C. C. Broadbridge, Z. Zhang, Y. Zhu, C. H. Ahn, and S. Ismail-Beigi, Interface-Induced Polarization and Inhibition of Ferroelectricity in Epitaxial $SrTiO_3$/Si, Phys. Rev. Lett. **105**, 217601 (2010).

[3] C. Battaglia, S. M. de Nicolás, S. D. Wolf, X. Yin, M. Zheng, C. Ballif, and A. Javey, Silicon heterojunction solar cell with passivated hole selective MoO_x contact, Appl. Phys. Lett. **104**, 113902 (2014).

[4] R. Islam, G. Shine, and K. C. Saraswat, Schottky barrier height reduction for holes by Fermi level depinning using metal/nickel oxide/silicon contacts, Appl. Phys. Lett. **105**, 182103 (2014).

[5] S. M. Sze and K. K. Ng, *Physics of Semiconductor Devices*, 3rd ed. (Wiley-Interscience, Hoboken, NJ, 2006).

[6] R. T. Tung, The physics and chemistry of the Schottky barrier height, Appl. Phys. Rev. **1**, 011304 (2014).

[7] W. Walukiewicz, Mechanism of Fermi-level stabilization in semiconductors, Phys. Rev. B **37**, 4760 (1988).

[8] J. L. Freeouf and J. M. Woodall, Schottky barriers: An effective work function model, Appl. Phys. Lett. **39**, 727 (1981).

[9] M. Schluter, Theoretical models of Schottky barriers, Thin Solid Films **93**, 3 (1982).

[10] J. Tersoff, Schottky Barrier Heights and the Continuum of Gap States, Phys. Rev. Lett. **52**, 465 (1984).

[11] C. A. Mead and W. G. Spitzer, Fermi level position at metal-semiconductor interfaces, Phys. Rev. **134**, A713 (1964).

[12] T. Iffländer, S. Rolf-Pissarczyk, L. Winking, R. G. Ulbrich, A. Al-Zubi, S. Blügel, and M. Wenderoth, Local Density of States at Metal-Semiconductor Interfaces: An Atomic Scale Study, Phys. Rev. Lett. **114**, 146804 (2015).

[13] R. Jaramillo and S. Ramanathan, Electronic granularity and the work function of transparent conducting ZnO:Al thin films, Adv. Funct. Mater. **21**, 4068 (2011).

[14] R. Gordon, Criteria for choosing transparent conductors, MRS Bull. **25**, 52 (2000).

[15] S.-H. Chen, C.-F. Yu, Y.-S. Lin, W.-J. Xie, T.-W. Hsu, and D. P. Tsai, Nanoscale surface electrical properties of aluminum zinc oxide thin films investigated by scanning probe microscopy, J. Appl. Phys. **104**, 114314 (2008).

[16] See Supplemental Material at http://link.aps.org/supplemental/10.1103/PhysRevApplied.6.034016 for details on sample preparation, measurement, and data analysis, which includes Refs. [17–30].

[17] P. J. Felfer, B. Gault, G. Sha, L. Stephenson, S. P. Ringer, and J. M. Cairney, A new approach to the determination of concentration profiles in atom probe tomography, Microsc. Microanal. **18**, 359 (2012).

[18] W. Gopel, Surface point defects and Schottky barrier formation on ZnO$(10\bar{1}0)$, J. Vac. Sci. Technol. **17**, 894 (1980).

[19] J.-H. Park, K.-J. Ahn, K.-I. Park, S.-I. Na, and H.-K. Kim, An Al-doped ZnO electrode grown by highly efficient cylindrical rotating magnetron sputtering for low cost organic photovoltaics, J. Phys. D **43**, 115101 (2010).

[20] K. Schulze, B. Maennig, K. Leo, Y. Tomita, C. May, J. Hüpkes, E. Brier, E. Reinold, and P. Bäuerle, Organic solar cells on indium tin oxide and aluminum doped zinc oxide anodes, Appl. Phys. Lett. **91**, 073521 (2007).

[21] A. Klein, C. Körber, A. Wachau, F. Säuberlich, Y. Gassenbauer, R. Schafranek, S. P. Harvey, and T. O. Mason, Surface potentials of magnetron sputtered transparent conducting oxides, Thin Solid Films **518**, 1197 (2009).

[22] G. B. Murdoch, S. Hinds, E. H. Sargent, S. W. Tsang, L. Mordoukhovski, and Z. H. Lu, Aluminum doped zinc oxide for organic photovoltaics, Appl. Phys. Lett. **94**, 213301 (2009).

[23] X. Jiang, F. L. Wong, M. K. Fung, and S. T. Lee, Aluminum-doped zinc oxide films as transparent conductive electrode for organic light-emitting devices, Appl. Phys. Lett. **83**, 1875 (2003).

[24] T. Kim, D. Choo, Y. No, W. Choi, and E. Choi, High work function of Al-doped zinc-oxide thin films as transparent conductive anodes in organic light-emitting devices, Appl. Surf. Sci. **253**, 1917 (2006).

[25] C. Huang, M. Wang, Z. Deng, Y. Cao, Q. Liu, Z. Huang, Y. Liu, W. Guo, and Q. Huang, Low content indium-doped zinc oxide films with tunable work function fabricated through magnetron sputtering, Semicond. Sci. Technol. **25**, 045008 (2010).

[26] K. Inoue, H. Takamizawa, Y. Shimizu, F. Yano, T. Toyama, A. Nishida, T. Mogami, K. Kitamoto, T. Miyagi, J. Kato, S. Akahori, N. Okada, M. Kato, H. Uchida, and Y. Nagai, Three-dimensional dopant characterization of actual metal–oxide–semiconductor devices of 65 nm node by atom probe tomography, Appl. Phys. Express **6**, 046502 (2013).

[27] K. Stiller, L. Viskari, G. Sundell, F. Liu, M. Thuvander, H.-O. Andrén, D. J. Larson, T. Prosa, and D. Reinhard, Atom probe tomography of oxide scales, Oxid. Met. **79**, 227 (2013).

[28] E. A. Marquis, B. P. Geiser, T. J. Prosa, and D. J. Larson, Evolution of tip shape during field evaporation of complex multilayer structures, J. Microsc. **241**, 225 (2011).

[29] F. Vurpillot, B. Gault, B. P. Geiser, and D. J. Larson, Reconstructing atom probe data: A review, Ultramicroscopy **132**, 19 (2013).

[30] W. R. McKenzie, E. A. Marquis, and P. R. Munroe, Focused ion beam sample preparation for atom probe tomography, in *Microscopy: Science, Technology, Applications And Education* (Formatex Research Center, Badajoz, 2010), pp. 1800–1810.

[31] J. G. Lu, S. Fujita, T. Kawaharamura, H. Nishinaka, Y. Kamada, T. Ohshima, Z. Z. Ye, Y. J. Zeng, Y. Z. Zhang, L. P. Zhu, H. P. He, and B. H. Zhao, Carrier concentration dependence of band gap shift in n-type ZnO:Al films, J. Appl. Phys. **101**, 083705 (2007).

[32] B. Hoffling, A. Schleife, C. Rödl, and F. Bechstedt, Band discontinuities at Si-TCO interfaces from quasiparticle calculations: Comparison of two alignment approaches, Phys. Rev. B **85**, 035305 (2012).

[33] K. B. Sundaram and A. Khan, Work function determination of zinc oxide films, J. Vac. Sci. Technol. A **15**, 428 (1997).

[34] V. Quemener, M. Alnes, L. Vines, P. Rauwel, O. Nilsen, H. Fjellvåg, E. V. Monakhov, and B. G. Svensson, The work function of n-ZnO deduced from heterojunctions with Si prepared by ALD, J. Phys. D **45**, 315101 (2012).

[35] H. Y. Kim, J. H. Kim, Y. J. Kim, K. H. Chae, C. N. Whang, J. H. Song, and S. Im, Photoresponse of Si detector based on n-ZnO/p-Si and n-ZnO/n-Si structures, Opt. Mater. **17**, 141 (2001).

[36] S. Lany and A. Zunger, Dopability, Intrinsic Conductivity, and Nonstoichiometry of Transparent Conducting Oxides, Phys. Rev. Lett. **98**, 045501 (2007).

[37] A. Bikowski, M. Rengachari, M. Nie, N. Wanderka, P. Stender, G. Schmitz, and K. Ellmer, Research update: Inhomogeneous aluminium dopant distribution in magnetron sputtered ZnO:Al thin films and its influence on their electrical properties, APL Mater. **3**, 060701 (2015).

[38] M. Xu, Y. Zhang, L. Wei, J. Zhang, B. Qian, J. Lu, C. Zhang, Y. Su, X. Dong, Y. Zhang, L. Wang, and X. Chen, Group III dopant segregation and semiconductor-to-metal transition in ZnO nanowires: A first principles study, RSC Adv. **3**, 19793 (2013).

[39] W. Körner and C. Elsässer, First-principles density functional study of dopant elements at grain boundaries in ZnO, Phys. Rev. B **81**, 085324 (2010).